



HAL
open science

Innovative ochre processing and tool use in China 40,000 years ago

Fa-Gang Wang, Shi-Xia Yang, Jun-Yi Ge, Andreu Ollé, Ke-Liang Zhao, Jian-Ping Yue, Daniela Eugenia Rosso, Katerina Douka, Ying Guan, Wen-Yan Li, et al.

► To cite this version:

Fa-Gang Wang, Shi-Xia Yang, Jun-Yi Ge, Andreu Ollé, Ke-Liang Zhao, et al.. Innovative ochre processing and tool use in China 40,000 years ago. *Nature*, 2022, 603 (7900), pp.284-289. 10.1038/s41586-022-04445-2. hal-03860971

HAL Id: hal-03860971

<https://hal.science/hal-03860971>

Submitted on 23 Oct 2023

HAL is a multi-disciplinary open access archive for the deposit and dissemination of scientific research documents, whether they are published or not. The documents may come from teaching and research institutions in France or abroad, or from public or private research centers.

L'archive ouverte pluridisciplinaire **HAL**, est destinée au dépôt et à la diffusion de documents scientifiques de niveau recherche, publiés ou non, émanant des établissements d'enseignement et de recherche français ou étrangers, des laboratoires publics ou privés.

1 To cite this article, please quote:” Wang, FG., Yang, SX., Ge, JY. *et al.* Innovative ochre processing and
2 tool use in China 40,000 years ago. *Nature* 603, 284–289 (2022). [https://doi.org/10.1038/s41586-022-](https://doi.org/10.1038/s41586-022-04445-2)
3 [04445-2](https://doi.org/10.1038/s41586-022-04445-2)”

4

5 **Innovative ochre processing and tool use in China ~40,000 years ago**

6 Fa-Gang Wang^{1†}, Shi-Xia Yang^{2,3,4,5†*}, Jun-Yi Ge^{2,3}, Andreu Ollé^{6,7}, Ke-Liang Zhao^{2,3}, Jian-
7 Ping Yue⁸, Daniela Eugenia Rosso^{9,10}, Katerina Douka^{4,11}, Ying Guan^{2,3}, Wen-Yan Li¹, Hai-
8 Yong Yang¹², Lian-Qiang Liu¹, Fei Xie¹, Zheng-Tang Guo¹³, Ri-Xiang Zhu¹⁴, Cheng-Long
9 Deng^{14,15*}, Francesco d'Errico^{16,17*}, Michael Petraglia^{4,18,19,20*}

10 ¹Hebei Provincial Institute of Cultural Relics and Archeology, Shijiazhuang 050031, China.

11 ²Key Laboratory of Vertebrate Evolution and Human Origins, Institute of Vertebrate
12 Palaeontology and Palaeoanthropology, Chinese Academy of Sciences, Beijing 100044, China.

13 ³Center for Excellence in Life and Palaeoenvironment, Chinese Academy of Sciences, Beijing
14 100044, China.

15 ⁴Department of Archaeology, Max Planck Institute for the Science of Human History, Jena
16 07745, Germany.

17 ⁵State Key Laboratory of Loess and Quaternary Geology, Institute of Earth Environment,
18 Chinese Academy of Sciences, Xi'an 710061, China.

19 ⁶Institut Català de Palaeoecologia Humana i Evolució Social (IPHES-CERCA), Zona
20 Educacional 4, Campus Sescelades URV (Edifici W3), 43007, Tarragona, Spain.

21 ⁷Universitat Rovira i Virgili, Dept. d'Història i Història de l'Art, Av. Catalunya 35, 43002,
22 Tarragona, Spain.

23 ⁸Department of History, Anhui University, Hefei 230039, China.

24 ⁹Université Côte d'Azur, CNRS, CEPAM, Nice, France.

25 ¹⁰Departament de Prehistòria, Arqueologia i Història Antiga, Grupo de Investigación Prehistoria
26 del Mediterráneo Occidental (PREMEDOC), Universitat de València, Valencia, Spain.

27 ¹¹Oxford Radiocarbon Accelerator Unit, Research Laboratory for Archaeology and the History
28 of Art, University of Oxford, Oxford, OX1 3TG, UK.

29 ¹²Museum of Yuzhou, Yuxian 075700, China.

30 ¹³Key Laboratory of Cenozoic Geology and Environment, Institute of Geology and Geophysics,
31 Chinese Academy of Sciences, Beijing 100029, China.

32 ¹⁴State Key Laboratory of Lithospheric Evolution, Institute of Geology and Geophysics, Chinese
33 Academy of Sciences, Beijing 100029, China.

34 ¹⁵College of Earth and Planetary Sciences, University of Chinese Academy of Sciences, Beijing
35 100049, China.

36 ¹⁶PACEA UMR 5199, Université de Bordeaux, CNRS, Pessac, France.

37 ¹⁷SFF Centre for Early Sapiens Behaviour (SapienCE), University of Bergen, Bergen, Norway.

38 ¹⁸Human Origins Program, National Museum of Natural History, Smithsonian Institution,
39 Washington, D.C. 20560, USA.

40 ¹⁹School of Social Science, The University of Queensland, Brisbane, Queensland 4072, Australia.

41 ²⁰Australian Research Centre for Human Evolution (ARCHE), Griffith University, Brisbane,
42 Australia.

43 †These authors contributed equally to this work.
44 * Corresponding authors. yangshixia@ivpp.ac.cn (S.X.Y.), cldeng@mail.iggcas.ac.cn (C.L.D.),
45 francesco.derrico@u-bordeaux.fr (F.D.), petraglia@shh.mpg.de (M.P.).

46
47
48 *Homo sapiens* was present in northern Asia by ~40,000 years ago, having ultimately replaced
49 archaic populations in Eurasia after episodes of earlier population expansions and
50 interbreeding¹⁻⁴. Cultural adaptations associated with the last Neanderthals, Denisovans and the
51 incoming populations of *H. sapiens* into Asia remain elusive^{1,5-7}. Here, we describe Xiamabei, a
52 well-preserved, ~40,000-year-old archaeological site in northern China, containing the earliest
53 known ochre processing feature in Eastern Asia together with a distinctive miniaturized lithic
54 assemblage, with bladelet-like tools bearing traces of hafting, and a bone tool. The cultural
55 assembly of traits at Xiamabei is unique for Eastern Asia and does not correspond with those
56 found at other archaeological site assemblages inhabited by archaic populations or to those
57 generally associated with the expansion of *H. sapiens*, such as the Initial Upper Palaeolithic⁸⁻¹⁰.
58 The record of northern Asia supports a process of cultural diversification and innovations
59 emerging in a period of hominin hybridization and admixture^{2,6,7,11}.

60

61

62 **Main Text**

63 One of the most profound events in human evolution was the worldwide expansion of *Homo*
64 *sapiens*^{1,5,12}. Fossil, genetic and archaeological evidence indicates that *H. sapiens* dispersed out
65 of Africa multiple times over the last ~200 thousand years (ka)^{1,13}, interbreeding with archaic
66 hominins, such as the Neanderthals and Denisovans as they migrated across Eurasia^{6,8,14}. Current
67 palaeoanthropological and archaeological evidence demonstrates that *H. sapiens* was present in
68 northern Asia by at least 40 ka ago²⁻⁴. It is often argued that the terrestrial expansion of modern
69 humans was facilitated by the use of advanced economic, social and symbolic adaptations
70 allowing occupation of a variety of ecosystems¹⁴. Pigment use, in particular, is seen as a key
71 indicator of symbolically mediated behaviour¹⁵⁻¹⁷, and technological innovations, such as the use
72 of miniaturised technology, is considered to have had adaptive and economic advantages^{18,19}.
73 Archaeological data, however, remain ambiguous as to the arrival of *H. sapiens* populations in
74 China (Supplementary Information A). With the exception of Initial Upper Palaeolithic (IUP)
75 and Mousterian toolkits in the Altai and Siberia, and a few sites in northern China²⁰⁻²², little is

76 known about stone tool industries in Eastern Asia until microblade assemblages become the
77 dominant technology after 29 ka^{9,23,24}. With respect to possible evidence for early symbolism,
78 only two engraved bones are known, one bearing residues of ochre, from northern China (ca.
79 125–105 ka), interpreted as the product of archaic hominins²⁵. Most artefacts signaling symbolic
80 practices are much younger, and likely linked to *H. sapiens*, such as pendants and ochre at
81 Zhoukoudian Upper Cave (ca. 35.1–33.5 ka)⁴ and beads at Shuidonggou 2 (SDG 2) (ca. 31 ka)²³.
82 Beads, pendants, and figurines become common after ca. 29 ka, when microblade technology
83 began to spread across northern China^{26–28}.

84 Here we report the results of archaeological findings at Xiamabei, a newly excavated and
85 well-preserved site in the Nihewan Basin of northern China (Fig. 1). Xiamabei contains the
86 earliest evidence of ochre processing, a novel miniaturized lithic technology, with bladelet-like
87 forms and hafted items, and a bone tool, dating to ~41–39 ka. Xiamabei stands apart from any
88 other known archaeological site in China as it possesses a novel set of cultural characteristics at
89 an early date. Located at the transition zone between the Inner Mongolian Plateau and North
90 China Plain, the site offers important new insights in the expansion of *H. sapiens* along the
91 northern route¹⁰.

92 Xiamabei is on the southern bank of the Huli River, where excavations were initiated in
93 2013 in the form of a trench exposing a 12 m² area (Supplementary Information B). The
94 stratigraphy, extending to a depth of 290 cm, encompasses six main layers in a floodplain
95 environment (Fig. 2). Layer 6, the main cultural horizon, 10–20 cm in thickness, is composed of
96 dark brown silty sediment, with occasional clay and sand aggregates. Layer 6 revealed evidence
97 for ochre use and processing, a charcoal-rich hearth, 382 miniaturized lithics, a single bone tool
98 (Extended Data Fig. 1) and 437 mammal bones (Fig. 1b–d). Characterization methods were
99 applied to sediment samples, ochre items, the bone tool, and a sample of the miniaturized lithics.
100 Accelerator mass spectrometry (AMS) ¹⁴C and optically stimulated luminescence (OSL) dating
101 yielded ages ranging between ca. 43 ka to 28 ka for the sequence, with the Layer 6 cultural
102 horizon dating to ca. 41–39 ka (Fig. 2, Supplementary Information C).

103 Pollen from Layer 6 indicates a steppe landscape with patches of coniferous forest
104 dominated by *Pinus*. The pollen assemblages and high *Artemisia*/Chenopodiaceae (A/C) ratio in
105 Layer 6 indicate a relatively cool and semi-arid climate during the site occupation
106 (Supplementary Information D). Faunal remains were highly fragmentary, with only 7.19%

107 being taxonomically identifiable. The presence of horse, deer and zokor is consistent with the
108 pollen evidence, reflecting a steppe landscape with patches of forest (Supplementary Information
109 D). The bulk of the mammalian fossils were less than 20 mm in length and most were burnt,
110 some even highly carbonized, suggesting their possible use as fuel (Supplementary Information
111 D2). Cutmarks were identified on two faunal fragments indicating that lithics were used to
112 process carcasses. A single bone tool bearing traces of use wear in the form of microflake scars
113 and polishing at one end, and regularization by scraping at the other end, possibly to facilitate
114 prehension or hafting, was recovered from Layer 6. The tool represents one of the earliest
115 examples in northern China for the working of bone with techniques proper to this raw material
116 (Extended Data Fig. 1).

117

118 **Ochre processing evidence**

119 Evidence for ochre processing at Xiamabei consists of three artefacts lying in close spatial
120 association and on a spot of red stained sediment whose colouration reduces in intensity on the
121 objects (Fig. 3, Extended Data Figs. 2–5, Supplementary Information E and F). The three
122 artefacts (Figs. 3a, b) consist of an ochre piece (OP1) consisting of an allochthonous hard iron-
123 rich nodule bearing clear traces of having been repeatedly abraded to produce a bright dark red
124 ochre powder (Fig. 3c), a smaller and more friable ochre piece (OP2) of a different composition
125 (Fig. 3d), resulting from crushing an original larger piece to produce ochre powder, and an
126 elongated limestone slab (LS) with smoothed areas stained with ochre (Fig. 3e) and preserving
127 residues of hematite-rich ochre (Fig. 3f) similar to that composing the smaller ochre piece. No
128 ochre residues were identified on an associated quartzite cobble (QC) bearing evidence of use as
129 a pestle (Fig. 3g).

130 X-ray diffraction (XRD), Micro Raman spectroscopy (MR), Micro-X-ray fluorescence
131 (Micro-XRF), mineral magnetism (MM), scanning electron microscopy coupled with energy
132 dispersive spectroscopy (SEM-EDS) were applied to 12 sediment samples from inside and
133 outside the red stained area on which the ochre pieces and associated artefacts were lying
134 (Extended Data Fig. 6, Supplementary Information G). In contrast to samples located at various
135 distances from the red stained area, two samples from inside the area are rich in FeO and contain
136 abundant microfragments of hematite-rich rocks. This indicates that the reddish colour of the

137 sediment (on which the stone artefacts and the ochre fragments were laying) is due to the
138 presence of diffuse ochre particles.

139 Taken together, the evidence indicates that different types of ochre were brought to the site
140 and processed using abrasion and pounding to produce ochre powder of different colour and
141 granulometry. Although the purpose of such an activity cannot be established (e.g., the
142 production of paint for colouring objects or decorating bodies, tanning of hides, using ochre as a
143 loading agent for adhesives), the quantity of ochre powder produced was large enough for the
144 leftover to permanently impregnate the sediment of the area on which tasks took place. This
145 work area, which represents the earliest known instance of ochre processing in Eastern Asia²⁸,
146 indicates that the use of this material was part of the behavioural repertoire of regional
147 populations by ~40 ka, preceding the origin of microblade technologies in China by 10,000 years.

148

149 **Novel miniaturized lithic assemblage with hafting evidence**

150 The Xiamabei lithic assemblage, composed of 382 artefacts, is a novel technology for northern
151 China, especially in consideration of its age. Most of the lithic artefacts (94%) are smaller than
152 40 mm and 58.37% (n=209) are smaller than 20 mm. Locally available small chert nodules and
153 quartz pebbles dominate the lithic assemblage, though porphyry pebbles were also sometimes
154 used. Freehand Hard Hammer Percussion (FHHP) and Bipolar Percussion (BP) methods were
155 the main reduction techniques, as shown by the coexistence of flake-cores with pronounced
156 Hertzian initiations and bipolar pieces with evidence of crushing on opposed platforms and
157 diffuse bulbs of percussion (Supplementary Information H). BP is the predominant reduction
158 technique, contributing to 70.11% of the identifiable specimens. The maximum length and width
159 of BP cores were not significantly smaller than the FHHP cores, indicating that although hand-
160 held flaking of small cores was possible, preference was given to bipolar reduction. Bipolar
161 splinters had an average width of 13.59 mm (29.5% smaller than 10 mm), falling within the
162 width range of formal microblades from younger sites in northern China²⁹. BP reduction
163 strategies therefore resulted in the efficient production of bladelet-like blanks that could be used
164 as tools, with lengths frequently measuring 20 mm or less (Fig. 4)³⁰.

165 In contrast to both earlier and contemporary lithic assemblages from the Nihewan
166 Basin^{31,32} retouched tools are exceedingly rare at Xiamabei. Only three pieces in the Xiamabei
167 assemblage show formal edge modification: two denticulates and one slightly retouched end-

168 scraper. Functional analysis conducted on a selected sample of lithics, including 13 bipolar and 4
169 FHHP products, identified use-wear on most of them (Supplementary Information D). Seven
170 pieces show clear evidence of hafting based on the arrangement of micro-scarring, the absence of
171 use-wear on areas covered by the hafting material, and the frequent presence of plant fiber
172 imprints, pointing to the use of binding elements (Fig. 4). Bone hafts have been identified in two
173 cases and exceptionally illustrated by a bladelet-like piece recovered with a portion of the haft
174 still in place (Fig. 4a, Extended Data Figs. 7–9). Wear patterns indicate the hafted pieces were
175 used for a variety of purposes including hide scraping, boring and scraping against hard matter
176 (likely wood), whittling soft plant material, and probably cutting soft animal matter. Two pieces
177 bearing an end-scraper outline were used in a manner consistent with classic Upper Palaeolithic
178 hide working tools, although only one of the implements showed formal distal retouch (Fig. 4b).
179 Use-wear on unhafted pieces complete the range of identified activities - mainly represented by
180 cutting actions on different materials, boring on a hard material, and in two cases, as wedges on
181 quartz flakes. Overall, the microscopic analyses indicated that the Xiamabei artefacts, including
182 bladelet-like tools manufactured by the BP technique, were used in a variety of activities
183 (Extended Data Fig. 10). In addition, ten artefacts with ochre residues, mainly in the form of
184 dispersed particles, were identified. On four pieces, residues were associated with the hafted area,
185 and on two pieces hide working was identified as residues were located on the active edge.
186 Ochre may have been used as an additive for hide working or as a loading agent for a hafting
187 adhesive.

188

189 **Implications for cultural adaptations in Eastern Asia**

190 The Xiamabei site excavations and analyses identifies the appearance, ~40,000 years ago, of new
191 cultural features that were either unknown or exceedingly rare in this region and in the
192 neighboring regions. The combination of two knapping techniques for the production of small
193 blanks, used for a variety of tasks and sometimes hafted, indicates the existence of a complex
194 technical system involving the use and transformation of different raw materials. Such a
195 technical system, not identified at older and penecontemporaneous sites, gives the Xiamabei
196 assemblage an original character. A workshop for the production and use of mineral pigments at
197 Xiamabei constitutes a second new cultural element in comparison with earlier and
198 contemporary sites. The use of ochre is not, however, associated with ostrich egg beads and

199 pierced teeth and shells found in younger sites, nor with the arrival, attested at younger sites, of
200 microblade technology. Although the taxonomic affiliation of the human group that occupied
201 Xiamabei ~40,000 years ago is not known, and an occupation by late Denisovans or even
202 Neanderthals cannot be excluded, the most parsimonious hypothesis, considering the presence of
203 contemporary fossils of modern humans at Tianyuandong², and somewhat younger at Salkhit³
204 and Zhoukoudian Upper Cave⁴, is that the visitors to Xiamabei were *H. sapiens*.

205 The way in which key cultural innovations emerged in different regions of the world
206 remains unclear. For some regions, such as Africa, a discontinuous and regionally variable
207 accretion model has been proposed, indirectly linked to the long and complex process that has
208 led to the emergence of our species in that continent³³. It has been argued that packages of
209 innovations originally developed in Africa or elsewhere may have been introduced by the spread
210 of modern humans into Eurasia. This is the model most often favoured for Asia, a region in
211 which, following European trends, blade and microblade technology, personal ornaments, ochre
212 use and complex bone technologies are seen as the signature of incoming *H. sapiens* populations.

213 The record emerging from northern China challenges dominant paradigms by showing
214 that during a critical time window, at ca. 40 ka, a variety of cultural adaptations existed. The
215 occurrence of a varied, though more simple lithic technology when compared to bladelet
216 production, associated with previously unrecorded hafting techniques, and the presence of some
217 innovations (ochre use, an expedient bone tool), and not others (formal bone tools, ornaments),
218 suggest that the cultural adaptations at Xiamabei may reflect a first colonisation by modern
219 humans, potentially involving cultural and genetic mixing with local Denisovans, and perhaps
220 replaced by a later second arrival. This supports the view that current evolutionary scenarios are
221 simplistic and that we should expect repeated but differential episodes of genetic and cultural
222 exchange over large geographic areas. We should also expect to identify a mosaic pattern
223 involving, in some instances, the spread of innovation packages, and in others, the persistence of
224 local traditions or the adoption of local invention of innovations with different rates of
225 complexities in technological and symbolic practices. This more complex evolutionary scenario
226 fits better with current biological and cultural evidence in comparison to one that envisions a
227 spread of innovation associated with a single, rapid wave of *H. sapiens* populations across
228 Eurasia.

229 **References**

- 230 1. Bae, C. J., Douka, K. & Petraglia, M. On the origin of modern humans: Asian perspectives. *Science* **358**,
231 1269–1269 (2017).
- 232 2. Fu, Q. et al. DNA analysis of an early modern human from Tianyuan Cave, China. *Proc. Natl. Acad. Sci. U.S.A.*
233 **110**, 2223–2227 (2013).
- 234 3. Massilani, D. et al. Denisovan ancestry and population history of early East Asians. *Science* **370**, 579–583
235 (2020).
- 236 4. Li, F., Bae, C. J., Ramsey, B., Chen, F. & Gao, X. Re-dating Zhoukoudian Upper Cave, northern China and its
237 regional significance. *J. Hum. Evol.* **121**, 170–177 (2018).
- 238 5. Timmermann, A. & Friedrich, T. Late Pleistocene climate drivers of early human migration. *Nature* **538**, 92–95
239 (2016).
- 240 6. Kuhlwilm, M. I. et al. Ancient gene flow from early modern humans into Eastern Neanderthals. *Nature* **530**,
241 429–433 (2016).
- 242 7. Bae, C. J. et al. Late Pleistocene human evolution in Eastern Asia behavioral perspectives. *Curr. Anthropol.* **58**,
243 514–526 (2017).
- 244 8. Hajdinjak, M. et al. Initial Upper Palaeolithic humans in Europe had recent Neanderthal ancestry. *Nature* **592**,
245 253–257 (2021).
- 246 9. Bar-Yosef, O. & Wang, Y. Palaeolithic Archaeology in China. *Annu. Rev. Anthropol.* **41**, 319–335 (2012).
- 247 10. Li, F., Petraglia, M., Roberts, P. & Gao, X. The northern dispersal of early modern humans in eastern Eurasia.
248 *Chin. Sci. Bull.* **65**, 1699–1701 (2020).
- 249 11. Dennell, R., Martínón-Torres, M., de Castro, J. M. B. & Gao, X. A demographic history of late Pleistocene
250 China. *Quat. Int.* **559**, 4–13 (2020).
- 251 12. deMenocal, P. B. & Stringer, C. Climate and the peopling of the world. *Nature* **538**, 49–50 (2016).
- 252 13. Harvati, K. et al. Apidima Cave fossils provide earliest evidence of *Homo sapiens* in Eurasia. *Nature* **571**,
253 500–504 (2019).
- 254 14. Dennell, R. *From Arabia to the Pacific: How Our Species Colonised Asia* (Routledge, London, ed. 1, 2020).
- 255 15. Hovers, E., Ilani, S., Bar-Yosef, O. & Vandermeersch, B. An early case of color symbolism: ochre use by
256 modern humans in Qafzeh Cave. *Curr. Anthropol.* **44**, 491–522 (2003).
- 257 16. Watts, I. Red ochre, body painting, and language: interpreting the Blombos ochre. *The Cradle of Language* **2**,
258 93–129 (2009).
- 259 17. Zipkin, A. M. *Material Symbolism and Ochre Exploitation in Middle Stone Age East-Central Africa* (Doctoral
260 dissertation, The George Washington University, 2015).
- 261 18. Villa, P. et al. Border Cave and the beginning of the Later Stone Age in South Africa. *Proc. Natl. Acad. Sci.*
262 *U.S.A.* **109**, 13208–13213 (2012).
- 263 19. Pargeter, J. & Shea, J. Going big versus going small: Lithic miniaturization in hominin lithic technology. *Evol.*
264 *Anthropol.* **28**, 72–85 (2019).
- 265 20. Zwyns, N. et al. The northern route for human dispersal in central and Northeast Asia: New evidence from the
266 site of Tolbor-16, Mongolia. *Sci. Rep.* **9**, 11759 (2019).
- 267 21. Peng, F., Lin, S. C., Patania, I. & Levchenko, V. A chronological model for the Late Paleolithic at Shuidonggou
268 Locality 2, North China. *PLoS ONE* **15**, e023268 (2020).
- 269 22. Li, F. et al. The easternmost Middle Paleolithic (Mousterian) from Jinsitai Cave, North China. *J. Hum. Evol.*
270 **114**, 76–84 (2018).
- 271 23. Li, F. et al. Chronology and techno-typology of the Upper Palaeolithic sequence in the Shuidonggou area,
272 northern China. *J. World Prehistory* **32**, 111–141 (2019).
- 273 24. Yue, J. et al. Human adaptations during MIS 2: Evidence from microblade industries of Northeast China.
274 *Palaeogeogr. Palaeoclimatol. Palaeoecol.* **567**, 110286 (2021).
- 275 25. Li, Z., Doyon, L., Li, H., Wang, Q. & d’Errico, F. Engraved bones from the archaic hominin site of Lingjing,
276 Henan Province. *Antiquity* **93**, 886–900 (2019).
- 277 26. Wei, Y., d’Errico, F., Vanhaeren, M., Peng, F. & Gao, X. A technological and morphological study of Late
278 Paleolithic ostrich eggshell beads from Shuidonggou, North China. *J. Archaeol. Sci.* **85**, 83–104 (2017).
- 279 27. Qu, T., Bar-Yosef, O., Wang, Y. & Wu, X. The Chinese Upper Paleolithic: Geography, Chronology, and
280 Techno-typology. *J. Archaeol. Res.* **21**, 1–73 (2013).
- 281 28. Martí, A. P., Wei, Y., Gao, X., Chen, F. & d’Errico, F. The earliest evidence of coloured ornaments in China:
282 The ochred ostrich eggshell beads from Shuidonggou Locality 2. *J. Anthropol. Archaeol.* **48**, 102–113 (2017).
- 283 29. Guan, Y. et al. Microblade remains from the Xishahe site, North China and their implications for the origin of
284 microblade technology in Northeast Asia. *Quat. Int.* **535**, 38–47 (2020).

- 285 30. Pargeter, J. & Faith, T. J. Lithic miniaturization as adaptive strategy: a case study from Boomplaas Cave, South
286 Africa. *Archaeol. Anthropol. Sci.* **12**, 225 (2020).
287 31. Guo, Y. J. et al. Luminescence ages for three ‘Middle Paleolithic’ sites in the Nihewan Basin, northern China,
288 and their archaeological and palaeoenvironmental implications. *Quat. Res.* **85**, 456–470 (2016).
289 32. Yang, S., Deng, C., Zhu, R. & Petraglia, M. The Paleolithic in the Nihewan Basin, China: Evolutionary history
290 of an Early to Late Pleistocene record in Eastern Asia. *Evol. Anthropol.* **29**, 125–142 (2020).
291 33. Scerri, E., Chikhi, L. & Thomas, M. Beyond multiregional and simple out-of-Africa models of human evolution.
292 *Nat. Ecol. Evol.* **3**, 1–3 (2019).
293

294 **Acknowledgements**

295 We thank Y. Lefrais (IRAMAT-CRP2A, UMR 5060 CNRS CNRS – Université Bordeaux-
296 Montaigne, France) and F. Orange (Université Côte d’Azur, Centre Commun de Microscopie
297 Appliquée, CCMA, Nice, France) for assistance with SEM-EDS analyses; A. Queffelec (PACEA
298 UMR 5199, University Bordeaux, CNRS, France) and L. Geis (PACEA UMR 5199, University
299 Bordeaux, CNRS, France) for assistance with the EDXRF analyses and the 3D imaging; C. X.
300 Zhang, B. Hu, M. L. Zhou, J. H. Li, Y. Liu, S. H. Yang, X. G. Li, Y. Chen, J. Yuan, Z. S. Shen,
301 S. Zhang and Z. X. Jiang (Institute of Geology and Geophysics, Chinese Academy of Sciences)
302 for assistance with the sediment analysis; B. Xu (Institute of Geology and Geophysics, Chinese
303 Academy of Sciences) and Y. Li (China University of Geosciences, Beijing) for discussions on
304 dating results; and R. P. Tang and F. X. Huan (Institute of Vertebrate Palaeontology and
305 Palaeoanthropology, Chinese Academy of Sciences) for assistance with figure preparation.

306 **Funding** Financial support for this research was provided by the National Natural Science
307 Foundation of China (41888101, 42177424, 41977380, 42072212 and 41690112), the Strategic
308 Priority Research Program of Chinese Academy of Sciences (XDB26000000), the Key Research
309 Program of the Institute of Geology & Geophysics, Chinese Academy of Sciences (IGGCAS-
310 201905), the State Key Laboratory of Loess and Quaternary Geology, Institute of Earth
311 Environment (SKLLQGZR2002), the Youth Innovation Promotion Association of Chinese
312 Academy of Sciences (2020074), the Humboldt Foundation, and the Max Planck Society. O.A.
313 was supported by the Spanish MICIU/Feder (PGC2018-093925-B-C32), the Catalan AGAUR
314 (SGR2017-1040) and the Univ. Rovira i Virgili (2019-PFR-URV-91) in the context of a MICIN
315 “María de Maeztu” excellence accreditation (CEX2019-000945). D.E.R. was funded by the
316 Fyssen Foundation, France, and the Juan de la Cierva-Formación Research Fellowship
317 (FJC2018-035605-I; Ministerio de Ciencia e Innovación, Spain). F.D. was funded by the
318 Research Council of Norway through its Centre of Excellence funding scheme (SFF Centre for
319 Early Sapiens Behaviour –SapienCE– project number 262618), the Talents program and the
320 GPR Human Past of the University of Bordeaux Initiative of Excellence. KD has received
321 funding from the ERC under the European Union’s Horizon 2020 research and innovation
322 program, grant agreement 715069-FINDER-ERC-2016-STG.

323 **Author contributions** F.G.W., S.X.Y., C.L.D, R.X.Z., Z.T.G., F.D.E. and M.P. obtained
324 funding and initiated the project; F.G.W., S.X.Y., J.Y.G, L.Q.L., F.X., Y. H.Y., Y.G. and W.Y.L.

325 conducted field excavation and site sampling; J.Y.G., K.L.Z., K.D. and C.L.D. conducted
326 stratigraphic and palaeoenvironmental studies; J.Y.G. performed the OSL dating; K.D.
327 performed the ¹⁴C dating; S.X.Y., J.P.Y., M.P. and A.O. analyzed the stone artefacts; F.D.E.,
328 D.E.R., Y.G. and C.L.D. analyzed the ochre processing artefacts and the sediment; and S.X.Y.,
329 C.L.D, F.D.E. and M.P wrote the main text and supplementary materials with specialist
330 contributions from the other authors.

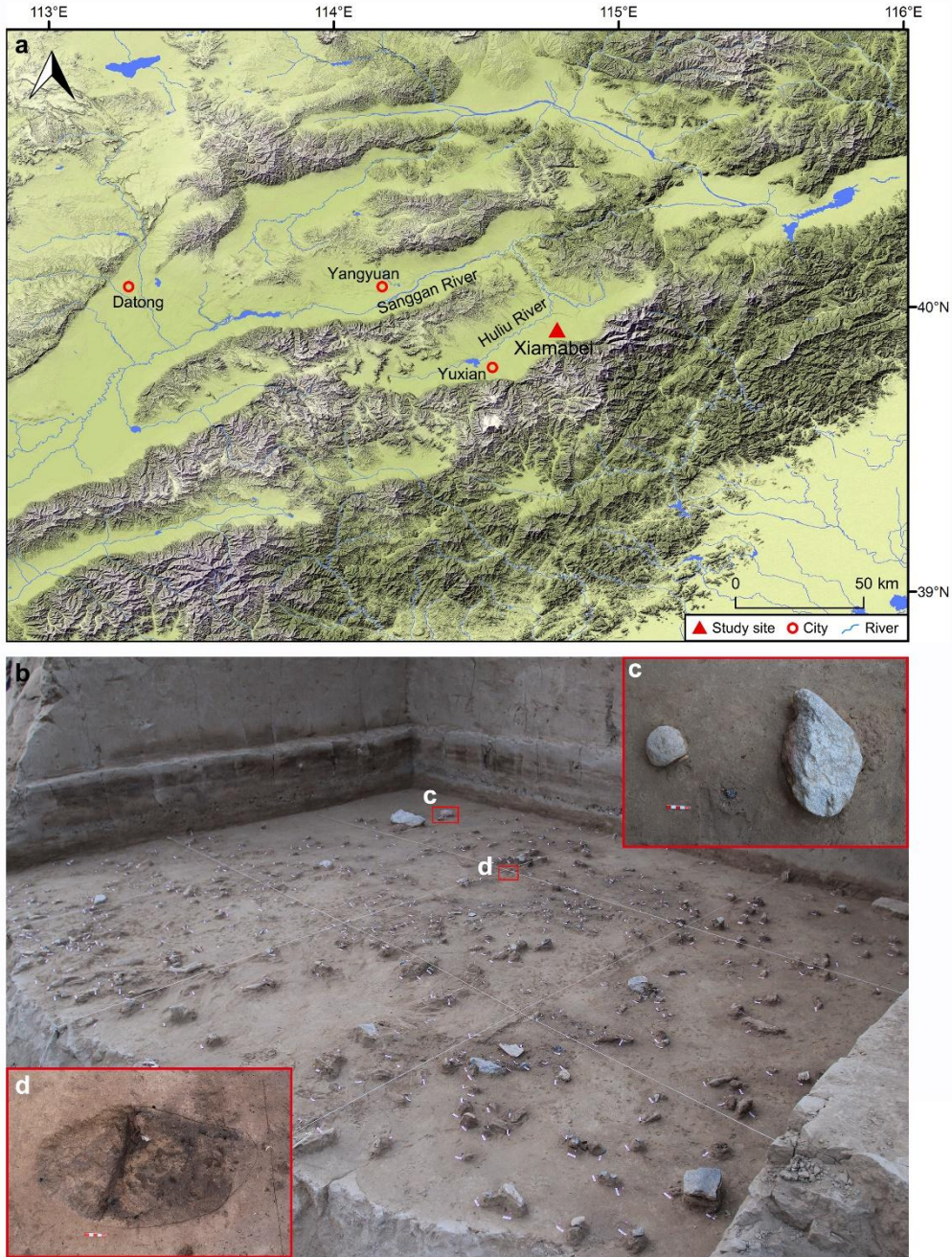
331 **Competing interests** The authors declare no competing interests.

332 **Data and materials availability** All relevant data are available in the main text or the
333 accompanying supplementary materials. All artefacts referred to in this study are curated in the
334 Institute of Vertebrate Palaeontology and Palaeoanthropology, Chinese Academy of Sciences,
335 Beijing, and Hebei Provincial Institute of Cultural Relics and Archeology in Shijiazhuang, China.
336 They are available for further research.

337 **Supplementary Materials**

338 Supplementary Information A–I

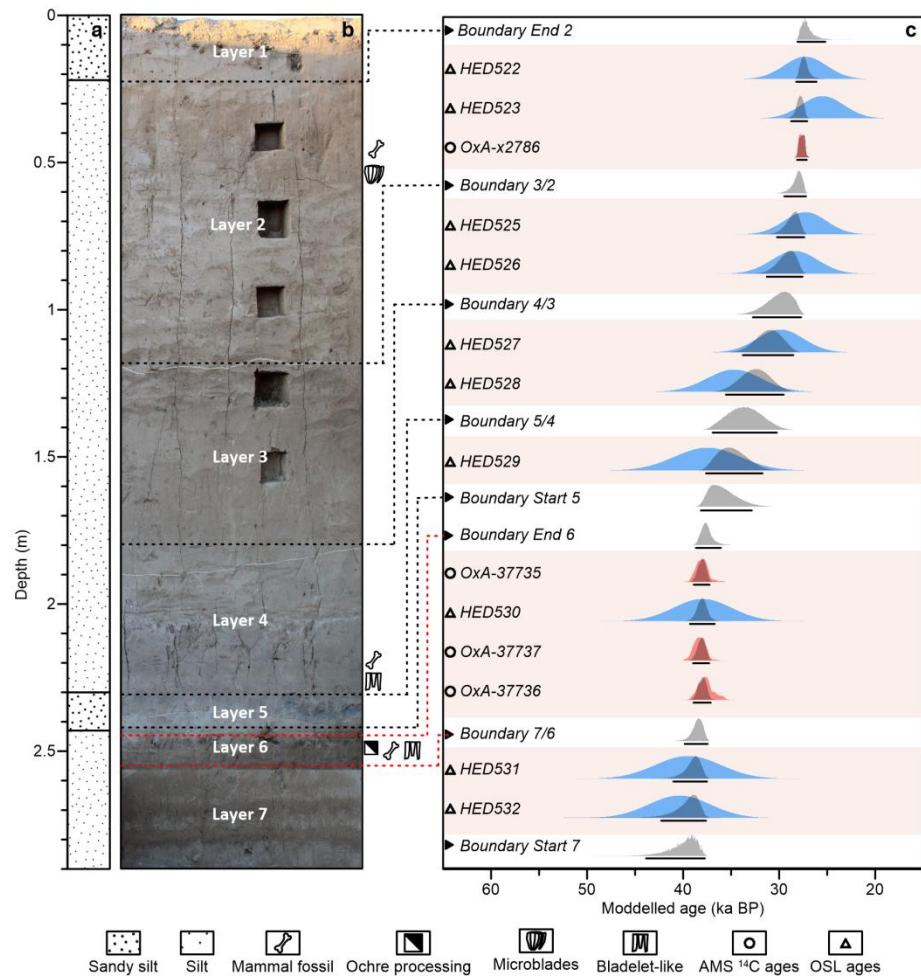
339 SI References



340

341 **Fig. 1 | Location of Xiamabei in the Nihewan Basin, China, and archaeological site**
 342 **excavations.** **a**, Location of Xiamabei in northern China, with regional map showing the
 343 location of the site on the south bank of the Huli River, Nihewan Basin. **b**, Distribution of
 344 cultural remains on the Layer 6 surface. **c**, Ochre processing feature showing a quartzite cobble
 345 (QC), an ochre piece (OP1) and a limestone slab (LS). **d**, View of the Layer 6 hearth, dated to
 346 ~41–39 ka.

347



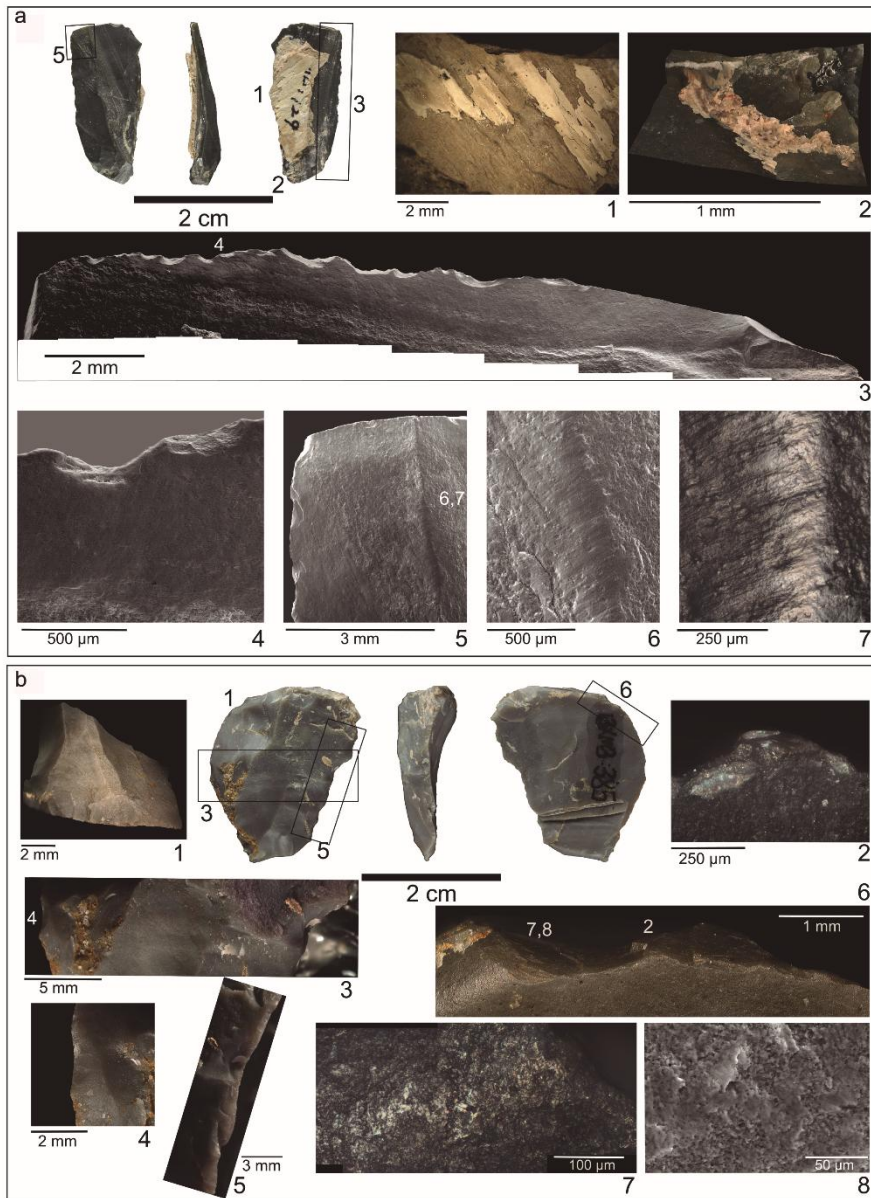
348

349 **Fig. 2 | Stratigraphy, sedimentary sequence and the position of luminescence and**
 350 **radiocarbon samples at Xiamabei. a, Main stratigraphic column. b, Layers identified in the**
 351 **field. c, Bayesian model of AMS ¹⁴C and OSL dates. The age probability distribution in blue, red**
 352 **and gray correspond to the OSL, AMS ¹⁴C and modelled ages, respectively.**



353

354 **Fig. 3 | Artefacts laying on the red stained sediment patch.** **a**, Quartzite cobble (QC),
 355 limestone slab (LS) and ochre piece (OP1) identified during the excavation. **b**, LS laying on an
 356 intense red stained sediment patch. **c**, Ochre piece modified by grinding (OP1). **d**, Ochre
 357 fragment probably resulting from crushing a larger ochre piece (OP2). **e**, LS showing ochre
 358 staining. **f**, Ochre microfragment (OMF) collected on the LS. **g**, Quartzite cobble (CG).



359

360 **Fig. 4 | Examples of use wear on lithics and residues on hafted pieces. a,** Bladelet-like piece
 361 with an adhering portion of the bone haft (no. 129); (1) detail of the bone; (2) imprints of plant
 362 fibers on calcium carbonate concretions likely related to binding; (3) ventral view of the active
 363 edge; (4-7) several details of the grit-influenced plant polish produced by a whittling action. **b,**
 364 End-scraper with punctual distal retouch (no. 385); (1) frontal view of the retouched area; (2)
 365 spot with ochre particles on the active distal end; (3-5) scarring and slight adequation on the
 366 hafted portion; (6-8) use wear produced by hide scraping. Images: a1-2 and b1, 3-6 3D Digital
 367 Microscope; a3-6, b8 Scanning Electron Microscope; a7, b2, 7 Reflected Light Optical
 368 Microscope.

369 **Methods**

370 **Radiocarbon dating**

371 Six animal bone fragments (all mammals) from Layers 2, 4 and 6 were collected and submitted
372 to the Oxford Radiocarbon Accelerator Unit (ORAU) for radiocarbon dating. The bones were
373 pretreated using routine methods for collagen extraction and purification, including an
374 ultrafiltration step, as described in Ramsey et al.³⁴ and Brock et al.³⁴.

375 The dates are reported in radiocarbon years BP (Before Present - AD 1950) using the half-
376 life of 5568 years. Isotopic fractionation was corrected for using the $\delta^{13}\text{C}$ values measured on the
377 AMS. The quoted $\delta^{13}\text{C}$ values are measured independently on a stable isotope mass spectrometer
378 (to ± 0.3 per mil relative to VPDB). The new ^{14}C determinations are calibrated using the
379 INTCAL20 calibration curve³⁶ and the OxCal 4.4 platform³⁷, with the age ranges in
380 Supplementary Information Table C1 expressed at the 95.4% confidence interval. The dating
381 report is included in Supplementary Information C1.

382 **Luminescence dating**

383 Dating of sediments using optically stimulated luminescence (OSL) signals in mineral grains was
384 first introduced by Huntley et al.³⁸. The OSL dating technique mostly determines the time
385 elapsed since the last sunlight exposure of a deposit, i.e., its burial time. The technique has been
386 widely used to date geological and archaeological deposits³⁹⁻⁴² in recent decades. The
387 luminescence emitted from minerals (e.g., quartz and feldspar) under artificial light exposure is
388 proportional to the absorbed energy accumulated within the crystal lattice of minerals by ionizing
389 radiation (e.g., alpha, beta or gamma radiation) from radioactive elements such as uranium (U),
390 thorium (Th), and potassium (K) in the environment, as well as cosmic rays^{40,43}. The total
391 luminescence of a sample which is often calibrated as a radiation dose (termed the equivalent
392 dose, De), is determined by comparing natural luminescence signals with signals yielded after a
393 known laboratory irradiation dose. Calculating the rate of natural irradiation (dose rate) at which
394 the sample absorbs energy from radiation in the environment during burial involves assessing the
395 radioactivity of the sample and its surroundings using chemical and radiometric methods, and
396 estimating the radiation contributed by cosmic rays. The luminescence age of sediments is then

397 achieved by subdividing the equivalent dose (Gy) by the dose rate (Gy/ka)⁴⁴.

398 A total of 10 sediment samples (Supplementary Information Table C3) was collected in the
399 Xiamabei sequence for OSL dating. All OSL samples were obtained by hammering steel tubes
400 (20 cm-long cylinders with a diameter of 5 cm) into a freshly dug vertical section. The tubes
401 were then covered and sealed with aluminum foil, and wrapped in black plastic bags and taped to
402 avoid light exposure and moisture loss. The sediment from the sunlight-exposed end of the
403 cylinder was separated and used for dose rate measurement. The material from the middle of the
404 cylinder was used for De measurement. Sample preparation, measurement and data analysis
405 procedures are described in Supplementary Information C2.

406 **Bayesian modelling and age of the Xiamabei section**

407 To establish the precise chronological framework of individual depositional units in Xiamabei,
408 we conducted Bayesian analysis that includes both the optical and ¹⁴C ages, using OxCal v4.4
409 ^{45–49}. All ¹⁴C ages were calibrated using the INTCAL 20 calibration curve. For each OSL age, we
410 used C date in calendar years before 2020 when the samples were collected with associated 1σ
411 errors as likelihood estimates. In order to harmonise the time the OSL was obtained and the
412 radiocarbon convention “BP=1950”, we subtracted 70 years from the OSL ages (2020–1950)
413 prior to them being modeled.

414 In order to estimate the posterior distributions (i.e., the modelled ages), the stratigraphic
415 order of each sample was input using the Sequence function (Supplementary Information Table
416 C4), based on the prior assumption that a sample stratigraphically lower is older than those above.
417 Samples that are from the same stratigraphic layer with similar depth, such as in Layer 6, were
418 modelled as a Phase, in which the measured ages are assumed to belong to same period. For the
419 layers with abrupt and clear boundaries between them, such as Layers 6 and 5, double (upper or
420 lower) boundaries were placed for them to constrain their start or end ages. Otherwise, for layers
421 which gradual stratigraphic changes were identified, assuming continuous sediment
422 accumulation, single transitional boundaries were placed between them. The samples, phases and
423 sequences were arranged according to their relative stratigraphic order.

424 To check for outliers, we applied the general t-type outlier model to detect outlier ages by
425 assessing the likelihood of each age being consistent with the modelled ages. A prior outlier
426 probability of 5% was assigned for the other samples with their posterior outlier probability

427 calculated during the modelling process. The CQL codes used to run the Bayesian model and
428 generate posterior age estimates are listed in Supplementary Information Table C5. The
429 generated probability distribution functions (PDF) for each of the samples are shown in Fig. 2
430 and their corresponding 95.4% probability ranges are summarized in Supplementary Information
431 Table C5. As demonstrated in Fig. 2, the Bayesian model results in a significant improvement of
432 the precision in age estimates for all the samples. None of the samples was flagged as an outlier,
433 as indicated by the posterior outlier probabilities, which are less than 4% for all samples. Using a
434 Date command we calculated the total span of each phase of interest, in particular, Layer 6 and
435 Layer 4. The model is shown in Supplementary Information C3.

436 **Ochre analysis**

437 Four artefacts were submitted to microscopic and geochemical analyses (Fig. 3): two ochre
438 pieces (OP1 and OP2, Extended Data Figs. 2,3), a quartzite cobble (QC, Extended Data Fig. 4)
439 and an elongated limestone slab (LS, Extended Data Fig. 5). During excavation, these four
440 artefacts were found in close spatial association (Fig. 3a) and lying on a large red stained
441 sediment spot (Fig. 3b). The cobble was cleaned under the microscope with a wet toothpick and
442 a soft brush. The recovered sediment was analysed to check the presence of phytoliths
443 (Supplementary Information F).

444 The four artefacts were examined with a motorised Leica Z6APOA microscope equipped
445 with a DFC420 digital camera and Leica Application Suite software (v.4.13, Wetzlar, Germany),
446 equipped with the Multifocus module and Leica Map DCM 3D computer software (6.2, Wetzlar,
447 Germany). The Multifocus module allows the acquisition of extended depth of field images by
448 relying on adapted algorithms that combine digital images collected at different heights into a
449 single, sharp, composite image. The obtained microscopic images were digitized and edited in
450 the Adobe® Photoshop® CS5.1 Extended software. The Leica Map DCM 3D allowed
451 production of 3D reconstructions of areas of interest on OP1.

452 Anthropogenic modifications on grindstones and ochre pieces were identified macro- and
453 microscopically. On grindstones, we recorded the presence of pits (depressions produced by a
454 pounding action), and smoothed areas (surfaces that have lost, comparatively to neighbouring
455 areas, irregularities and projections through abrasive action)⁵⁰⁻⁵². On ochre pieces, we identified
456 polished areas (shiny surfaces that may have been produced by use or by rubbing against a soft

457 surface), striations (linear parallel marks arranged in groups produced by grinding the piece
458 against an abrasive surface), and facets (flat areas covered with striations produced by grinding
459 an object on a flat, hard abrasive surface)^{53–55}.

460 An ochre microfragment (OMF, Fig. 3f; Extended Data Fig. 5) adhering to the surface of
461 the limestone slab LS (zone 1 in Extended Data Fig. 5a) was removed with a scalpel under the
462 microscope without producing any damage to the artefact and put on a carbon adhesive tab
463 adhering to a SEM stub.

464 Scanning Electron Microscopy (SEM) observations and Energy Dispersive X-Ray
465 spectroscopy (EDS) analyses on OP1 and OP2 were conducted with a JEOL IT 500 HR
466 instrument equipped with two EDS Oxford Instruments Ultimex 100 spectrometers. Both
467 samples were observed under the same magnifications ($\times 60$, $\times 1000$, $\times 3000$, $\times 4000$ and in a few
468 cases $\times 10,000$) (Supplementary Information E). EDS analyses and backscattered electron images
469 (BSE) were obtained under low vacuum mode at a pressure of 30 Pa with a 20 kV accelerating
470 voltage. SEM observations and EDS analyses on sample OMF were conducted with a Tescan
471 Vega3 XMU scanning electron microscope (TESCAN FRANCE, Fuveau, France) equipped with
472 an Oxford X-MaxN 50 EDS detector (Oxford Instruments, Abingdon, U.K). A 10 kV
473 accelerating voltage was used for imaging using secondary and backscattered electrons, and 20
474 kV for EDS analyses. All samples were observed with no prior metal or carbon coating. All EDS
475 spectra were processed with the Aztec software (version 3.1, Oxford Instruments, UK).

476 μ -Raman (μ -RS) analyses were conducted to determine the mineralogical composition of
477 OP1, OP2 and sample OMF, using a SENTERRA Dispersive Raman Microscope (Bruker)
478 equipped with an internal calibration system. The working area was examined using an
479 integrated colour camera. Spectra were acquired with a 785 nm laser and a laser power of 1 to 10
480 mW. The spectra were recorded with an integration time varying from 5 to 10 s, in a spectral
481 range from 100 to 2200 cm^{-1} , with a number of co-additions varying between 5 to 10 depending
482 on the presence of fluorescence radiation and signal-to-noise ratio. Data was collected with the
483 OPUS 7.2 software package (Bruker, Billerica, USA). Mineral identification was based on the
484 comparison of the recorded spectra with those of available in the RRUFF spectra library,
485 University of Arizona⁵⁶.

486 The elemental composition of OP1 and OP2 was established by energy dispersive X-ray
487 fluorescence (EDXRF) (Extended Data Fig. 6). Measurements were acquired using a positioning

488 device consisting of a metallic receptacle to which the spectrometer was fixed. Sample OMF was
489 not analysed because its size is smaller than the spectrometer aperture (3x4 mm in diameter)⁵⁷.
490 EDXRF measurements were performed with a portable SPECTRO xSORT X-ray fluorescence
491 spectrometer from Ametek, equipped with a silicon drift detector (SDD), a W X-ray tube with an
492 excitation source set at 40 kV, 0.1 mA. Spectra acquisition times were set to 120 s. The
493 spectrometer is internally calibrated by an automated measure of the elemental composition of a
494 standard metal shutter. A supplementary calibration^{58,59}, based on the Lucas-Tooth and Price
495 methodology, was applied⁶⁰. This calibration, developed with the X-labpro software (Ametek,
496 Berwyn, USA) adjusts the mass attenuation coefficient and calibration slopes for major and trace
497 elements by using certified standards and reference samples analysed by ICP-OES and ICP-MS.
498 The Ochre analysis results in details can be found in Supplementary Information E.

499 **Sediment analysis**

500 Twelve sediment samples, as listed in Supplementary Information Table G1, were selected for
501 mineralogical, elemental and magnetic analysis. Two samples (X1 and X2) come from the red
502 stained area on which the ochre fragments OP1 and OPI2, limestone slab LS and cobble QS were
503 found (Extended Data Fig. 10), two samples (X3 and X6) were retrieved in the same layer but at
504 ca. 2 m far from the stained area, eight other (X4, X5, XMB2101–XMB2106) were collected
505 between 20 and 200 m far from the excavated area (Supplementary Information Fig. G1). All the
506 samples consist of floodplain silt.

507 XRD analysis⁶¹ was carried out on the twelve samples (Supplementary Information Table
508 G1), using a Netherland PANalytical X'PerPRO diffractometer with the following parameters:
509 Ni-filtered Cu-K α /40kV/40mA, scattering slit of 1/16°, receiving slit of 5 mm, continuous scan
510 mode, scanning speed of 0.049884°/s, and a scanning step of 0.0167113°. Bulk minerals were
511 identified based on the following peaks: quartz, 4.26 Å; anorthoclase, 3.21 Å; albite, 3.18 Å;
512 rutile, 3.189 Å; calcite, 3.03 Å; dolomite, 2.89 Å; Hematite, 2.70 Å; Koninckite, 8.42 Å; and clay
513 minerals smectite/chlorite, 14.1 Å; illite, 10.0 Å. The relative proportions of the identified
514 minerals were roughly determined using their peak intensities by measuring the heights of the
515 main reflections with PANalytical X'pert HighScore software (Version 2.2e).

516 Raman spectra^{61,62} were obtained with a Witec alpha300R confocal-Raman spectrometer
517 equipped with a solid-state continuous-wave laser emitting at 532 nm, and diffraction gratings of

518 300 grooves mm^{-1} . A piece of single-crystal silicon was used to calibrate the wavenumbers of
519 the shifts. Laser focusing and sample viewing are performed through a Zeiss microscope fitted
520 with an EC Epiplan 50 \times objective lens (NA=0.75). The spot size is less than 1 μm and the
521 resolution is 4.8 cm^{-1} . The laser power impinging on the hematite single crystal was 0.40 mW. A
522 spectra acquisition time of 30 s and total spectra with 20 accumulations were collected for each
523 measurement.

524 Non-destructive Micro-XRF analyses were performed on the twelve sediment samples
525 (Supplementary Information Table G1) following the procedures of Li et al.⁶³. The Micro-XRF
526 measurements were carried out on the M4 TORADO PLUS Micro-XRF analyzer. One area of
527 about 0.5–1 cm^2 for each sample was randomly selected for collecting the XRF signals with the
528 same measuring parameters (e.g., 50 kV of high voltage, 600 μA of anode current, 20 μm of spot
529 size, 10 μm of pixel size, and 20 ms/pixel of pixel time). For semi-quantitative comparisons,
530 each XRF spectrum was normalized with the signal of the Rh-La peak, which is generated by a
531 Rh X-ray source. The data were analyzed with the M4 TORNADO Bruker Microanalysis
532 Software.

533 Mineral magnetic measurements were made on the twelve sediment samples
534 (Supplementary Information Table G1) in order to determine the magnetic mineralogy^{64–71}. χ - T
535 curves were obtained by continuous exposure of samples through temperature cycles from room
536 temperature to 700°C and back to room temperature with a ramping rate of 2°C/min, using an
537 AGICO MFK1-FA equipped with CS-3 temperature control system. To minimize the possibility
538 of oxidation, the samples were heated and cooled in an argon atmosphere. For each sample, we
539 subtracted the contribution of the sample holder and thermocouple to the magnetic susceptibility.
540 Hysteresis loops were measured using a MicroMag 3900 Vibrating Sample Magnetometer (VSM)
541 (Princeton Measurements Corp., USA). The magnetic field was cycled between ± 1.5 T for each
542 sample. Saturation magnetization (M_s), saturation remanence (M_r), and coercivity (B_c) were
543 determined after the correction for the paramagnetic contribution identified from the slope at
544 high fields. Samples were then demagnetized in alternating fields up to 1.5 T, and an isothermal
545 remanent magnetization (IRM) was imparted from 0 to 1.5 T also using the MicroMag 3900
546 VSM. Subsequently the IRM at 1.5 T was demagnetized in a stepwise backfield from 0 to -1.5 T
547 to obtain coercivity of remanence (B_{cr}). Magnetic component analyses of coercivity distributions
548 were analyzed using the IRM-CLG program of Kruiver et al.⁶⁶.

549 To better constrain the origin and microstructure of the sediment, selected samples (X1, X2,
550 X4, X6) were observed using optical microscopy and analysed using Scanning Electron
551 Microscopy (SEM) coupled with Energy Dispersive X-Ray spectroscopy (EDS). Backscattered
552 electron microscopy analyses were conducted using a scanning electron microscope with an
553 energy dispersive spectrometer (JSM-IT500).

554 Detailed results of the sediment analyses can be found in Supplementary Information G.
555

556 **Stone tool functional and residue analysis**

557 The stone tool functional analysis is based on the fundamentals of traceology⁷²⁻⁷⁴, which has
558 been subsequently consolidated, systematized⁷⁵⁻⁷⁹ and strengthened to improve interpretation^{76,77}.
559 The study applied criteria established experimentally⁸⁰⁻⁸⁴, incorporating a multi-scalar approach
560 and a multi-technique microscopic analysis⁷⁵⁻⁸⁸. Potential residues were characterized
561 microscopically, including study of their elementary chemical composition, without removing
562 adhering materials from tools⁸⁹⁻⁹².

563 Use-wear and residues were documented with the combined use of Optical Microscopy
564 (OM), Scanning Electron Microscopy (SEM) and 3D Digital Microscopy (3D DM). Four main
565 procedures (I-IV) were used for analysis.

566 I) A preliminary assessment of the samples and the location of features of special interest
567 was conducted. This was conducted at low magnification, using a stereomicroscope (Euromex
568 DZ.1105), with a magnification range of 8×-80× (0.8×-8× zoom, 10× oculars), and equipped
569 with a 20MP 1” Scemex camera (Horizontal Field of View 16.6 mm -1.67 mm).

570 II) A systematic screening at different magnifications using 3D DM (Hirox KH-8700) was
571 conducted. This microscope is equipped with a dual illumination revolver zoom lens (MXG-
572 5000REZ) which together with the high intensity LED light source allows for the observation of
573 samples with a 5700 K color temperature. This lens consists of a triple objective turret with a
574 different zoom range per objective, allowing for magnifications ranging from 35 to 5000×
575 (HFOV 8.6 mm–60 μ). The microscope is equipped with a high-sensitivity compact CCD camera
576 that enabled the capture of 24 frames per second at high resolution (1600×1200 pixels). The dual
577 illumination system allows for the observation of sample topography with ring and coaxial light.

578 The former is suitable for the observation of topographical irregularities with a uniform even
579 illumination at low magnifications, while coaxial light serves to highlight the topography of flat
580 surfaces at high magnifications. Ring and coaxial lights were used individually and even
581 combined, according to the observation conditions required by the samples. The interest of this
582 microscope lies on its integrated stacking and stitching technology, capable of performing real-
583 time 2D and 3D tiltings and generating wide field of view images of large surface areas which, in
584 turn, create quantifiable 3D models.

585 III) More conventional observations were conducted with a reflected light microscope. We
586 used a Zeiss Axio Scope A.1 metallographic microscope, with differential interference contrast
587 (DIC) system involving a Nomarsky interference contrast filter. The microscope was equipped
588 with 10× oculars and objectives EC Epiplan ranging from 5×/0.13 to 50×/0.5 HD DIC, resulting
589 in nominal magnifications ranging from 50 to 500 times. Pictures were taken with a 6.3 MP 1.8”
590 FLIR camera, and fully focused images were obtained through a motorized stage and Winkoms
591 Encoder Z 1.0 and Helicon Focus 5.3 software. Resulting HFOV ranges from 2.9mm to 295µm.

592 IV) An environmental SEM (ESEM FEI Quanta 600 model) with an energy dispersive X-
593 ray spectrometer (EDX-EXL II System analytical oxford) for microanalysis, equipped with an
594 INCA software (v 4.01) from Oxford Instruments for digital image acquisition, was conducted.
595 Most observations were carried out between 60× and 2000× (HFOV 6.9 mm to 207 µ, 24”
596 display). Observations were entirely done in low vacuum mode (LV), so the coating of the
597 samples with conductive materials (gold or carbon) was not required. Large field (LFD) and
598 back-scattered electron detectors (DualBSD) were used in combination to observe residues and
599 use-wear features.

600 Sample processing based on protocols tested in previous studies^{79,87} were adapted in our
601 microscopic workflow. No cleaning was applied during first observations; a very soft cleaning
602 was performed prior to the characterization of residues by OM, 3D DM or SEM analysis; and, a
603 more thorough cleaning was subsequently applied when necessary, to document use-wear
604 features in detail. The main cleaning steps were: 1) Removal of the ink and varnish used to mark
605 the archaeological tools with acetone; 2) 5 to 15 min ultrasonic baths in a 2% neutral phosphate-
606 free detergent solution (Derquim®); 3) 5 min baths in hydrogen peroxide (H₂O₂, 130vol) to
607 remove modern organic matter, when spotted; 4) Removal of residues from cleaning products
608 under running water; 5) 2–5 min ultrasonic baths in pure acetone to remove any residues from

609 handling. When necessary, 5 min baths in a 10% HCl solution were applied to remove
610 carbonated residues. Before each observation, tools were dried with compressed air to avoid
611 contact with the laboratory paper and to reduce the formation of liquid spots on the surface,
612 which may lead to misleading interpretations. During the entire process, samples were handled
613 using powder-free gloves and plastic tweezers.

614 Experimental reference collections available at the IPHES Lithic Technology Laboratory,
615 derived from published and ongoing programs, were used to compare to the Xiamabei results,
616 thereby assisting in interpretations. The experimental programs involved actions on a range of
617 common contact materials, and artefacts made on a variety of raw materials, including chert,
618 quartzite, quartz, limestone, basalt, and obsidian^{83–85,88,90,91,93–97}. Interpretations were also
619 supported by information supplied in the wider literature. Detailed reporting on the Xiamabei
620 samples is provided in Supplementary Information I.

621

622

- 623 34. Ramsey, B. C., Higham, T. & Leach P. Towards high-precision AMS: Progress and limitations.
624 *Radiocarbon* **46**, 17–24 (2004).
- 625 35. Brock, F., Higham, T., Ditchfield, P. & Ramsey C. B. Current pretreatment methods for AMS radiocarbon
626 dating at the Oxford Radiocarbon Accelerator Unit (ORAU). *Radiocarbon* **52**, 103–112 (2010).
- 627 36. Reimer, P. et al. The IntCal20 Northern Hemisphere radiocarbon age calibration curve (0–55 cal kBP).
628 *Radiocarbon* **62**, 725–757 (2020).
- 629 37. Bronk, C. B. Bayesian analysis of radiocarbon dates. *Radiocarbon* **51**, 337–360 (2009).
- 630 38. Huntley, D. J., Godfrey-Smith, D. I. & Thewalt, M. L. W. Optical dating of sediments. *Nature* **313**, 105–
631 107 (1985).
- 632 39. Duller, G. Distinguishing quartz and feldspar in single grain luminescence measurements. *Radiat. Meas.*
633 **37**, 161–165 (2003).
- 634 40. Rhodes, E. J. Optically stimulated luminescence dating of sediments over the past 200,000 years. *Annu.*
635 *Rev. Earth Planet. Sci.* **39**, 461–488 (2011).
- 636 41. Zhang, X. L. et al. The earliest human occupation of the high-altitude Tibetan Plateau 40 thousand to 30
637 thousand years ago. *Science* **362**, 1049–1051 (2018).
- 638 42. Ge, J. Y. et al. Evidence from the Dayao Palaeolithic site, Inner Mongolia for human migration into arid
639 northwest China during mid-Pleistocene interglacials. *Quat. Res.* **103**, 113–129.
- 640 43. Duller, G. Luminescence dating of Quaternary sediments: Recent advances. *J. Quat. Sci.* **19**, 183–192
641 (2004).
- 642 44. Aitken, M. J. *Introduction to Optical Dating: The Dating of Quaternary Sediments by the Use of Photon-*
643 *Stimulated Luminescence* (Clarendon Press, 1998).
- 644 45. Ramsey, B. C. Deposition models for chronological records. *Quat. Sci. Rev.* **27**, 42–60 (2008).
- 645 46. Ramsey, B. C. Bayesian analysis of radiocarbon dates. *Radiocarbon* **51**, 337–360 (2009).
- 646 47. Ramsey, B. C. Dealing with outliers and offsets in radiocarbon dating. *Radiocarbon* **51**, 1023–1045 (2009).
- 647 48. Ramsey, B. C. *Bayesian Approaches to the Building of Archaeological Chronologies* (CRC Press Boca
648 Raton, FL, 2015).
- 649 49. Ramsey, B. C. Methods for summarizing radiocarbon datasets. *Radiocarbon* **59**, 1809–1833 (2017).
- 650 50. Adams, J. et al. “Functional analysis of macro-lithic artefacts” in Non-Flint Raw Material Use in
651 Prehistory: Old Prejudices and New Directions, F. Sternke, L. Eigeland, L.J. Costa, Eds. (Archaeopress,

- 2009), pp. 43–66.
- 653 51. de Beaune, S. *Pour une archéologie du geste: Broyer, moudre, piler, des premiers chasseurs aux premiers*
654 *agriculteurs* (CNRS Editions, 2000).
 - 655 52. Rosso, D. E., Mart, í A. P. & d' Errico, F. Middle Stone Age ochre processing and behavioural complexity
656 in the Horn of Africa: Evidence from Porc-Epic Cave, Dire Dawa, Ethiopia. *PLoS ONE* **11**, e0164793
657 (2016).
 - 658 53. Hodgskiss, T. Identifying grinding, scoring and rubbing use-wear on experimental ochre pieces. *J.*
659 *Archaeol. Sci.* **37**, 3344–3358 (2010).
 - 660 54. Rifkin, R. F. Processing ochre in the Middle Stone Age: Testing the inference of prehistoric behaviours
661 from actualistically derived experimental data. *J. Anthropol. Archaeol.* **31**, 174–195 (2012).
 - 662 55. Rosso, D. E., d'Errico, F. & Queffelec, A. Patterns of change and continuity in ochre use during the late
663 Middle Stone Age of the Horn of Africa: the Porc-Epic Cave record. *PLoS ONE* **12**, e0177298 (2017).
 - 664 56. Lafuente, B., Downs, R. T., Yang, H. & Stone N. “The power of databases: the RRUFF project” in
665 Highlights in Mineralogical Crystallography, T. Armbruster, R. M. Danisi, Eds. (W. De Gruyter, 2015) pp.
666 1–30.
 - 667 57. Bassel, L. et al. Fluorescence-based knife-edge beam diameter measurement to characterize X-ray beam
668 profiles in reflection geometry. *Spectroc. Acta Pt. B-Atom. Spectr.* **118**, 98–101 (2016).
 - 669 58. Dayet, L. et al. Manganese and iron oxide use at Combe-Grenal (Dordogne, France): A proxy for cultural
670 change in Neanderthal communities. *J. Archaeol. Sci. Rep.* **25**, 239–256 (2019).
 - 671 59. Queffelec, A., d'Errico, F. & Vanhaeren, M. “Analyse des blocs de matière colorante de Praileaitz I (Deba,
672 Gipuzkoa)” in Munibe Monographs ([Anthropology and Archaeology Series](#), 2017). pp. 493–503.
 - 673 60. Lucas-Tooth, H. J. and Price, B. J. A mathematical method for the investigation of inter-element effects in
674 X-ray fluorescence. *Metallurgia* **64**, 149–152 (1961).
 - 675 61. Anthony, J. W., Bideaux, R. A., Bladh, K. W. & Nichols, M. C. *Handbook of Mineralogy* (Mineral Data
676 Publishing, Tucson Arizona, USA, 1990).
 - 677 62. Hanesch, M. Raman spectroscopy of iron oxides and (oxy)hydroxides at low laser power and possible
678 applications in environmental magnetic studies. *Geophys. J. Int.* **17**, 941–948 (2009).
 - 679 63. Li, J. H. et al. Micro-XRF study of the troodontid dinosaur *Jianianhualong Tengi* reveals new biological
680 and taphonomical signals. *Atomic Spectroscopy* **42**, 1–11 (2021).
 - 681 64. Deng, C., Zhu, R., Jackson, M. J., Verosub, K. L. & Singer, M. J. Variability of the temperature-dependent
682 susceptibility of the Holocene eolian deposits in the Chinese loess plateau: a pedogenesis indicator. *Phys.*
683 *Chem. Earth (A)* **26**, 873–878 (2001).
 - 684 65. Dunlop, D. J. & Özdemir Ö. *Rock Magnetism: Fundamentals and Frontiers* (Cambridge Univ. Press,
685 Cambridge, UK, 1997).
 - 686 66. Kruiver, P. P., Dekkers, M. J. & Heslop, D. Quantification of magnetic coercivity components by the
687 analysis of acquisition curves of isothermal remanent magnetization. *Earth Planet. Sci. Lett.* **189**, 269–276
688 (2001).
 - 689 67. Jiang, Z. et al. Ferro and antiferromagnetism of ultrafine-grained hematite. *Geochem. Geophys. Geosyst.*
690 **15**, 2699–2712 (2014).
 - 691 68. Özdemir, Ö. & Dunlop, D. J. Hysteresis and coercivity of hematite. *J. Geophys. Res. Solid Earth* **119**,
692 2582–2594 (2014).
 - 693 69. Roberts, A. P., Cui, Y. & Verosub, K. L. Wasp-waisted hysteresis loops: mineral magnetic characteristics
694 and discrimination of components in mixed magnetic systems. *J. Geophys. Res.* **100**, 17909–17924 (1995).
 - 695 70. Yuan, J. et al. Rapid drift of the Tethyan Himalaya terrane before two-stage India-Asia collision. *Natl. Sci.*
696 *Rev.* **8**, nwaal73, doi:10.1093/nsr/nwaa173 (2021).
 - 697 71. Roberts, A. P. et al. Hematite (α -Fe₂O₃) quantification in sedimentary magnetism: limitations of existing
698 proxies and ways forward. *Geosci. Lett.* **7**, 8, doi:10.1186/s40562-020-00157-5 (2020).
 - 699 72. Semenov, S. A. *Prehistoric Technology. An Experimental Study of the Oldest Tools and Artefacts From*
700 *Traces of Manufacture and Wear* (Cory, Adams and Mackay Ltd., London, 1964).
 - 701 73. Hayden, B. (Ed), *Lithic Use-Wear Analysis* (Academic Press, New York, 1979).
 - 702 74. Keeley, L. H. *Experimental Determination of Stone Tools Uses: A Microwear Analysis* (The University of
703 Chicago Press, Chicago, 1980).
 - 704 75. Vaughan, P. C. *Use-Wear Analysis of Flaked Stone Tools* (The University of Arizona Press, Tucson, 1985).

- 705 76. Knutsson, K. Patterns of tools use. Scanning electron microscopy of experimental quartz tools (Societas
706 Archaeologica Upsalensis, Uppsala, 1988), vol. 10.
- 707 77. González, J. E. & Ibáñez, J. J. *Metodología de Análisis funcional de instrumentos tallados en sílex*
708 (Universidad de Deusto, Bilbao, 1994)
- 709 78. Levi Sala, I. *A Study of Microscopic Polish on Flint Implements* (Tempus Reparatum, Oxford, 1996). BAR
710 IS629.
- 711 79. Marreiros, J. M., Gibaja Bao, J. F. & Ferreira Bicho, N. *Use-Wear and Residue Analysis in Archaeology*
712 (Springer Cham Heidelberg New York, 2015).
- 713 80. Stemp W. J., Watson A. S. & Evans A. A. Surface analysis of stone and bone tools. *Surf. Topogr. Metrol.*
714 *Prop.* **4**, 13001 (2016).
- 715 81. Ollé, A. & Vergès, J. M. “SEM functional analysis and the mechanism of microwear formation” in
716 ‘Prehistoric Technology’ 40 years later: Functional Studies and the Russian Legacy. Proceedings of the
717 International Congress Verona (Italy), 20-23 April 2005, Longo L., Skakun N., Eds. (Archaeopress,
718 Oxford, 2008), BAR 1783, pp. 39–49.
- 719 82. Ollé, A. & Vergès, J. M. The use of sequential experiments and SEM in documenting stone tool microwear.
720 *J. Archaeol. Sci.* **48**, 60–72 (2014).
- 721 83. Fernández-Marchena, J. L. & Ollé, A. Microscopic analysis of technical and functional traces as a method
722 for the use-wear analysis of rock crystal tools. *Quat. Int.* **424**, 171–190 (2016).
- 723 84. Pedergrana, A. & Ollé, A. Monitoring and interpreting the use-wear formation processes on quartzite
724 flakes through sequential experiments. *Quat. Int.* **427**, 35–65 (2017).
- 725 85. Borel, A., Ollé, A., Vergès, J. M. & Sala, R. Scanning Electron and Optical Light Microscopy: two
726 complementary approaches for the understanding and interpretation of usewear and residues on stone tools.
727 *J. Archaeol. Sci.* **48**, 46–59 (2014).
- 728 86. Ollé, A. et al. Microwear features on vein quartz, rock crystal and quartzite: a study combining Optical
729 Light and Scanning Electron Microscopy. *Quat. Int.* **424**, 154–170 (2016).
- 730 87. Pedergrana, A., Ollé, A. & Evans, A. A. A new combined approach using confocal and scanning electron
731 microscopy to image surface modifications on quartzite. *J. Archaeol. Sci. Rep.* **30**, 102237 (2020).
- 732 88. Martín-Viveros, J. I. & Ollé, A. Use-wear and residue mapping on experimental chert tools. A multi-scalar
733 approach combining digital 3D, optical, and scanning electron microscopy. *J. Archaeol. Sci. Rep.* **30**,
734 102236 (2020).
- 735 89. Monnier, F., Ladwig, J. & Porter, L. S. T. Swept under the rug: the problem of unacknowledged ambiguity
736 in lithic residue identification. *J. Archaeol. Sci.* **39**, 3284–3300 (2012).
- 737 90. Pedergrana, A., Asryan, L., Fernández-Marchena, J. L. & Ollé, A. Modern contaminants affecting
738 microscopic residue analysis on stone tools: A word of caution. *Micron* **86**, 1–21 (2016).
- 739 91. Pedergrana, A. & Ollé, A. Building an experimental comparative reference collection for lithic micro-
740 residue analysis based on a multi-analytical approach. *J. Archaeol. Method Theory* **25**, 117–154 (2018).
- 741 92. Xhaufclair, H. et al. Use-related or contamination? Residue and use-wear mapping on stone tools used for
742 experimental processing of plants from Southeast Asia. *Quat. Int.* **427**, 80–93 (2017).
- 743 93. Martín-Viveros, J. I. & Ollé, A. Using 3D digital microscopy and SEM-EDX for in-situ residue analysis: A
744 multi-analytical contextual approach on experimental stone tools. *Quat. Int.* **569–570**, 228–262 (2020).
- 745 94. Hayes, E., Cnuts, D. & Rots, V. Integrating SEM-EDS in a sequential residue analysis protocol: Benefits
746 and challenges. *J. Archaeol. Sci. Rep.* **23**, 116–126 (2019).
- 747 95. Ollé, A. Variabilitat i patrons funcionals en els sistemes tècnics de Mode 2. Anàlisi de les deformacions
748 d’ús en els conjunts lítics del Riparo Esterno de Grotta Paglicci (Rignano Garganico, Foggia), Áridos
749 (Arganda, Madrid) i Galería-TN (Sierra de Atapuerca, Burgos). Thesis, Universitat Rovira i Virgili,
750 Tarragona (2003).
- 751 96. Fernández-Marchena, J. L. et al. Rainbow in the dark. The identification of diagnostic projectile impact
752 features on rock crystal. *J. Archaeol. Sci. Rep.* **31**, 102315 (2020).
- 753 97. Martín-Viveros, J. I. et al. Use-wear analysis of a specific mobile toolkit from the Middle Palaeolithic site
754 of Abric Romaní (Barcelona, Spain): a case study from level M. *Archaeol. Anthropol. Sci.* **12**, 16 (2020).
- 755 98. Downs, R.T. **The RRUFF Project: an integrated study of the chemistry, crystallography, Raman and**
756 **infrared spectroscopy of minerals.** Program and Abstracts of the 19th General Meeting of the International
757 Mineralogical Association in Kobe, Japan. p. 3–13. (2006).

- 758 99. Robertson, D. J. & France, D. E. Discrimination of remanence-carrying minerals in mixtures, using
759 isothermal remanent magnetisation acquisition curves. *Phys. Earth Planet. Inter.* **82**, 223–234 (1994).
760 100. Swanson-Hysell, N. L., Fairchild, L. M. & Slotznick, S. P. Primary and secondary red bed
761 magnetization constrained by fluvial intraclasts. *J. Geophys. Res. Solid Earth* **124**, 4276–4289 (2019).
762